

# Forest Structure Estimation using POLInSAR

Shane Cloude<sup>(1)</sup>, Karin Viergever<sup>(2)</sup>, Iain H Woodhouse<sup>(2)</sup>

<sup>(1)</sup> AEL Consultants, Cupar, Fife, SCOTLAND, UK, [aclc@mac.com](mailto:aclc@mac.com)

<sup>(2)</sup> School of Geosciences (Geography), University of Edinburgh, SCOTLAND, UK, [i.h.woodhouse@ed.ac.uk](mailto:i.h.woodhouse@ed.ac.uk)

## Abstract

In this paper we provide a review of progress in our development of new forest parameter retrieval algorithms using advanced polarimetric modes of the ALOS-PALSAR radar sensor. We first summarize data availability for our test sites in Scotland and Belize before giving details of our latest processing algorithms. Our approach is based on an eigenvector analysis of the scattering coherency matrix and we use this to both classify different forest types and via an eigenvector filtering approach, to estimate physical parameters. Finally we show some sample results obtained from ALOS-PALSAR

**Keywords:** Radar Polarimetry, Forest Parameter Estimation.

## 1. INTRODUCTION

Our project is concerned with the development of new quantitative remote sensing techniques for forestry applications. In particular we are interested in the use of fully coherent imaging polarimetry (POLSAR) and repeat-pass polarimetric SAR interferometry (POLInSAR) from the L-band PALSAR sensor. We are investigating a range of potential techniques across different forest environments, ranging from biomass and its relation to forest height estimation, through structure parameterization to forest regrowth dynamics and hydrology issues.

To help validate our new algorithms we employ data from two scientific test sites, both supported by existing L-band airborne radar databases in both polarimetric and polarimetric interferometry modes, as well as by extensive in-situ measurements of forest properties. Due to sensor schedule conflicts, we have not been able to acquire any repeat pass POLInSAR data over our sites but have obtained several POLSAR images. Hence in this report we concentrate on using this data to illustrate the clear advantages of using full quadpol L-band data for quantitative work in forestry applications.

## 2. DESCRIPTION OF TEST SITES AND DATA

Our three primary test sites are summarised in table 1. We have two in the north of Scotland, representing mountainous semi-natural pine and plantation pine environments. The third is located in Belize in the Caribbean, where there is a diverse range of tropical forest environments available for study. The main reason for selecting these sites is the availability to our group of

supporting L-band airborne data (from JPL-AIRSAR for Belize and DLR E-SAR for Scotland). There is also extensive support from in-situ measurements of forest parameters, in Scotland provided by Forest Research and in Belize by the NGO operated Rio Bravo Conservation and Management Area (RBCMA) via its long-term contacts with the University of Edinburgh [1].

Table 1 : Forest Test Site Locations

Forest Site	Location	Type
Glen Affric	5°W, 57°N	Semi-natural Pine
Cairngorm	3.8°W, 57°N	Plantation Pine
Belize	88°W 17°N	Tropical Mixed

Table 2 : PALSAR Quadpol Data Availability

Forest Site	PALSAR Mode	Acquisition Dates
Glen Affric	PLR21.5	16/10/06 + 15/03/07
Cairngorm	PLR21.5	15/03/07
Belize	PLR21.5	20/09/06 + 5/11/06

Table 2 summarises our site acquisitions up to 15/11/07. To date we have received no suitable interferometric pairs for these sites and hence cannot yet consider POLInSAR analyses (such as forest height estimation). Instead we turn to consider in more detail our progress in exploiting single pass polarimetric or POLSAR data.

## 3. POLSAR PROCESSING METHODOLOGY

To counter image speckle effects, we begin by performing multi-look averaging of the SLC quad-pol data. Consequently we do not obtain a direct estimate of the pixel scattering matrix  $[S]$  itself but instead its 4x4 Hermitian coherency matrix  $\langle[T]\rangle$  (note that we employ all four channels of polarimetric data instead of the three demanded of backscatter reciprocity. This enables a more consistent treatment of noise and calibration errors in space borne systems). In order to retrieve the scattering matrix for a given pixel we therefore employ an eigenvector decomposition of  $\langle[T]\rangle$  as shown in equation 1 [2]. In this study we select the eigenvector  $\underline{e}_1$  corresponding to the dominant eigenvalue ( $\lambda_1$ ) as our candidate scattering matrix. Several secondary parameters can then be derived from the full eigenvalue spectrum, most notably the scattering entropy  $H$ , [2] that we employ for forest/nonforest discrimination. In the next

stage, we extract the scattering alpha parameter of the dominant eigenvector [6,7].

$$\begin{aligned} \langle [T] \rangle &= \lambda_1 \underline{e}_1 + \lambda_2 \underline{e}_2 + \lambda_3 \underline{e}_3 + \lambda_4 \underline{e}_4 \\ \lambda_1 &\geq \lambda_2 \geq \lambda_3 \geq \lambda_4 \geq 0 \end{aligned} \quad (1)$$

From symmetry arguments, we expect only a mixture of symmetric scattering mechanisms to occur in forestry [3]. Equation 2 shows how we can then derive an estimate of  $\alpha_s$ , the symmetric component of the alpha parameter.

$$\underline{e}_1 = \begin{bmatrix} \cos \alpha \\ \sin \alpha \cos \beta e^{i\delta} \\ \sin \alpha \sin \beta e^{i\chi} \end{bmatrix}$$

$$\xrightarrow{\text{Cameron}} \underline{e}_{1s} + \underline{e}_{ns} = \begin{bmatrix} \cos \alpha_s \\ \sin \alpha_s \cos \beta_s e^{i\delta} \\ \sin \alpha_s \sin \beta_s e^{i\delta} \end{bmatrix} + \underline{e}_{ns} \quad (2)$$

$$\underline{e}_{1s} = \begin{bmatrix} 1 & 0 & 0 \\ 0 & \cos \beta_s & -\sin \beta_s \\ 0 & \sin \beta_s & \cos \beta_s \end{bmatrix} \begin{bmatrix} \cos \alpha_s \\ \sin \alpha_s e^{i\delta_s} \\ 0 \end{bmatrix}$$

We start with the dominant unitary eigenvector and first extract the maximum symmetric component of the eigenvector using a Cameron decomposition [3]. Finally we obtain a 2 dimensional complex unit vector, which has two parameters,  $\alpha_s$  and a phase  $\delta_s$  as shown in equation 2. These two can be considered spherical coordinates of a point on the surface of a unit sphere, called the alpha sphere. This sphere maps all possible symmetric scattering matrices and will be used to isolate different scattering mechanisms in our image. We also define a convenient polar projection of this sphere onto a plane, called the alpha plane. Here the outer circle represents the equator of the alpha sphere and upper and lower semi-circles represent positive and negative alpha values (note that the sign of  $\alpha$  depends on the phase angle  $\delta$ . As a simple example, if  $HH > VV$  then  $\delta$  will be 0 while if  $VV > HH$  then  $\delta = \pi$ ). Note that this alpha plane is a more complex construct than the usual alpha-entropy diagram used in POLSAR classification [2]. We now turn to consider how to use this representation to estimate parameters in forest scattering.

#### 4. FOREST PARAMETER ESTIMATION USING POLSAR DATA

In our approach we estimate parameters directly from the polarized dominant eigenvector for each pixel. In particular we are interested in exploiting dihedral or double bounce scattering in forest environments. However rather than using it to maximise RCS and map seasonal flooding for example, we plan to exploit fully polarimetric data to use this mechanisms to estimate

trunk dielectric constant (and hence water content) as follows. We start by considering a triplet of polarizing scattering mechanisms, as shown in figure 1

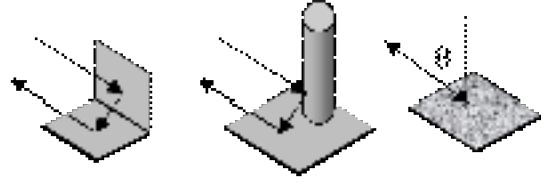


Figure 1: Three Primary Scattering Mechanisms leading to Polarized Radar returns

In addition, there will generally also be some volume scattering effects from random foliage etc. but this will be largely filtered by our eigenvalue technique and hence we can concentrate on these three as primary source of polarized returns in the imagery. Importantly, for the spaceborne geometry of PALSAR, we can separate these in the data as follows Starting with the simpler case of surface Bragg scatter on the right of figure 1, it is well known that the alpha magnitude increases (negatively) with increasing  $\epsilon_r$  [2,3]. However it has low sensitivity for small  $\theta$ , for example a change in dielectric constant from 10 to 20 causes a change of only 1 degree in alpha. Hence the polarized surface scattering response in ALOS imagery will be very limited on the alpha sphere. However, when vegetation is present there exists the possibility of dihedral scattering with very different properties as follows.

Turning now to dihedral scattering (considering only the dual-Fresnel case on the left in figure 1 for illustration), we find we have a potential ambiguity, in that we have two dielectric constants to consider, one for each surface. However, for small angles of incidence, the primary dependence comes from the second and not the first reflection. This can be qualitatively explained because the first surface is always illuminated at a small angle, for which the Fresnel reflection coefficients are almost equal in HH and VV, while the second surface is illuminated at a much larger angle (to make the total reflection 180 degrees or backscatter). Indeed the second angle can be so large as to approach the Brewster angle, which represents a phase transition in polarimetry terms with 180 degrees HH/VV phase before and zero phase beyond the Brewster angle. For this reason the alpha parameter for dihedral scattering (contrary to usual interpretations [3]) can lie below  $\pi/4$ . Figure 2 shows an example. Here we show the variation of alpha with dielectric constant of the second surface (for  $\epsilon_r = 10$  for the first). We show results for three angles of incidence, 23,24 and 25 degrees (covering the swath of ALOS-PALSAR) and see only a small change. We see that as dielectric constant increases so alpha increases, but in contrast to surface scatter we see much higher sensitivity. For example, if the dielectric constant changes from 10

to 20 we have a change in alpha of 10 degrees, an order of magnitude larger than for the direct surface case.

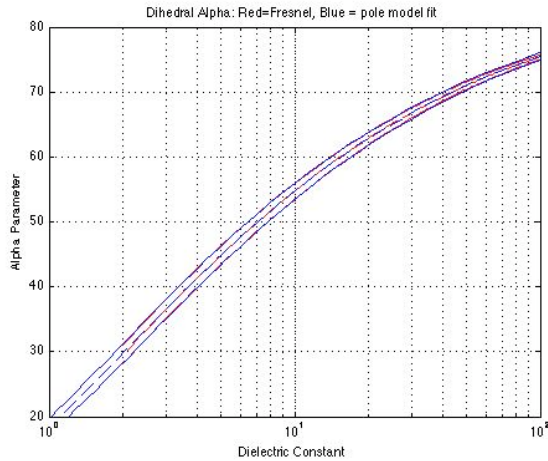


Figure 2: Relation between alpha and stem dielectric constant for angles of incidence from 23 to 25 degrees

Note however that we are sensitive to different dielectric constants in the two cases. In the direct surface case we are sensitive to changes in the surface dielectric directly. In the second however we have little or no sensitivity to this term and instead sense changes in the dielectric constant of the second reflection, which in vegetation applications will be the plant stem dielectric. Figure 3 summarises these two very different scattering mechanisms, direct and dihedral, on the alpha plane. Here we see that direct surface scattering always has a negative alpha (VV > HH) while the dihedral has a positive alpha (HH > VV) and a phase shift of 180 degrees for dielectric constants greater than 5 (the Brewster angle corresponding to which is 66 degrees, matching the 24 degree incidence angle of ALOS).

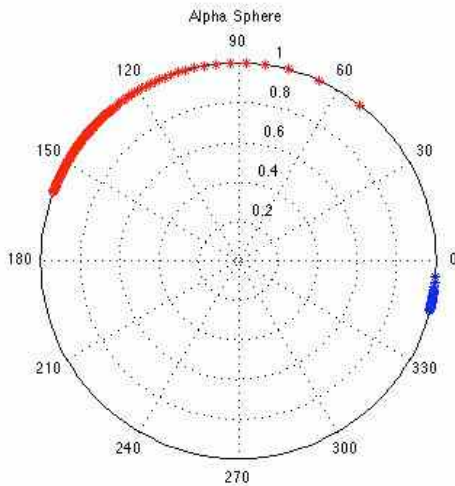


Figure 3: Dihedral (red) and Surface (blue) scattering alpha parameter plotted on the alpha plane for  $\theta = 24^\circ$

We note that the two mechanisms are clearly separated on the alpha plane for this angle of incidence and hence

we can easily identify which type of polarized scattering is occurring in SAR imagery by locating the dominant eigenvector on this diagram. We can also use figure 2 to relate alpha directly to dielectric constant using a curve fit. One key feature of the fit must be that when  $\alpha$  tends to  $\pi/2$  so  $\epsilon_r$  tends to infinity (a metallic dihedral has an alpha of  $\pi/2$  [3]) and hence the function must have a pole at  $\pi/2$ . We then obtain the following fit from figure 2 (fitting  $\theta = 24$  degrees as the middle of the swath).

$$\epsilon_r \approx \frac{3.2299}{\left(\frac{\pi}{2} - \alpha_s\right)^{2.5}} - 0.8522 \quad - (3)$$

This relation then enables us to estimate the dielectric constant of the second reflection inside the vegetation. At L-band, this second reflection comes primarily from the trunk of trees in a forest and hence we have a potential method for remotely estimating the wood dielectric constant of trees. The problem is that not all forests provide a suitably polarized signal (a large dominant eigenvalue in equation 1). In dense forests dominated by volume scattering this signal can be very small and the eigenvalue spectrum relatively flat. However, we have found from ALOS data that in more open woodlands, as occurs for example in tropical savannah regions in Belize, there is a strongly polarized signal to be exploited. Such regions are an important area of study for space borne remote sensing, making up 40% of the tropics and 15% of the earth's surface. We now turn to show some initial results of this approach applied to ALOS data.

#### 4. EXPERIMENTAL RESULTS

Figure 4 shows an example of using the eigenvalue spectrum for improved forest/non-forest classification. In the upper part we show a conventional HH SAR image of the Glen Affric region in Scotland. We note the poor contrast between forest and open moorland. In the lower image we show a colour entropy/alpha [2] composite from polarimetric PALSAR data and here we see the blue polarized scattering from open moorland in contrast to the forested regions, with a flatter eigenvalue spectrum, higher entropy and less saturated colour. Turning now to the polarized behaviour of savannah woodland, we show in figure 5 a colour composite of our test area in Belize. We also show a range line sample crossing through the dense primary forest and into the open savanna woodland and the corresponding eigenvalue spectra. Here we see that the polarized return is only 50 or 60% in the primary forest but can rise to over 80% in the savannah. Finally in figure 7 we show the set of pixels where the polarization is greater than 80% and which lie in the dihedral scattering region of figure 3. In red (yellow) we show those points with high (low) dielectric constant from figure 2. The high density of points in the savanna area is encouraging for our application. The next step in our project will be to validate these points as isolated tree locations in our test area and

establish their correlation with ground truth.

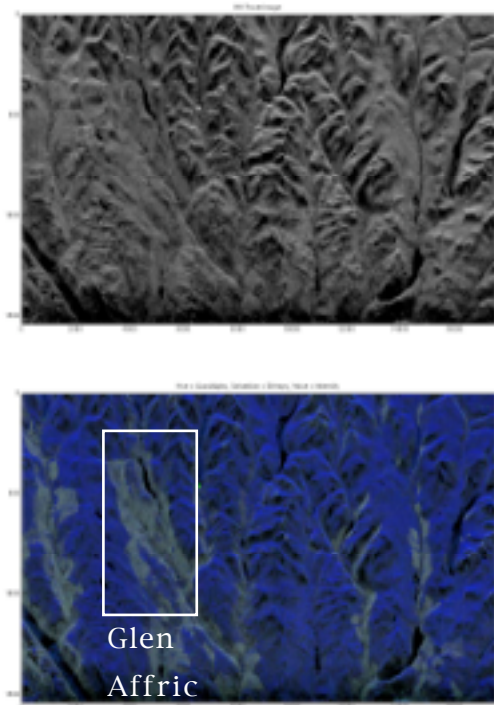


Figure 4. HH PALSAR Image (upper) and Entropy/alpha composite (lower) for Glen Affric test site

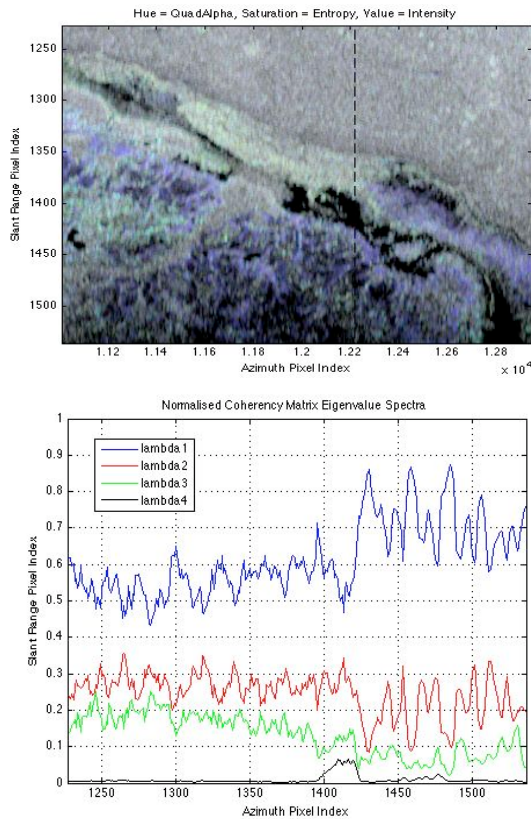


Figure 5 : Entropy/Alpha Image of Belize test site (upper) and sample eigenvalue spectra variation for a range line

(lower)

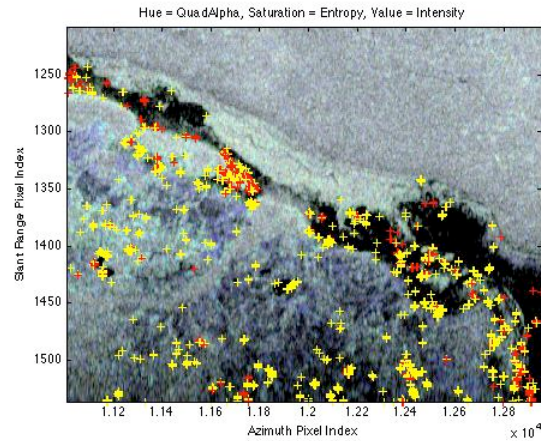


Figure 6 : Entropy/Alpha Image of Belize site with pixels highlighted where the degree of polarization is greater than 80% and where dihedral scattering occurs

## 5. DISCUSSION AND CONCLUSIONS

In this paper we have demonstrated a new application of L-band polarimetric radar imagery for quantitative forest parameter estimation. We have shown how an eigenvalue approach to POLSAR processing can provide not only improved land use classification products, but also important parameter sets. In our example we have shown how to exploit the polarized component of radar returns to isolate dihedral scattering in open woodlands. We have shown how to use the polarimetric parameters of this component to estimate trunk dielectric constant. Future studies will concentrate on validation of the algorithms and, according to data availability, to look at multitemporal issues related to fire regrowth and seasonal changes.

### Acknowledgement

This research is conducted under the agreement of JAXA Research Announcement entitled 'Polarimetric Radar Interferometry for the Quantitative Estimation of Forest Structure' (JAXA-PI 007).

### References

- [1] K. Viergever et al. 2006. SAR remote sensing for natural resource management – using online GPS services as control for detailed ground truthing. *Geomatics World*, 4(14):32-37.
- [2] S.R. Cloude, E. Pottier, "An Entropy Based Classification Scheme for Land Applications of Polarimetric SAR", *IEEE Transactions on Geoscience and Remote Sensing*, Vol. 35, No. 1, pp 68-78, January 1997
- [3] S.R. Cloude, E. Pottier, "A Review of Target Decomposition Theorems in Radar Polarimetry", *IEEE Transactions on Geoscience and Remote Sensing*, Vol. 34 No. 2, pp 498-518, March 1996